Carbohydrate Polymers 168 (2017) 346–355

Contents lists available at ScienceDirect

Carbohydrate Polymers

journal homepage: www.elsevier.com/locate/carbpol

Optical sensor platform based on cellulose nanocrystals (CNC) – 4′-(hexyloxy)-4-biphenylcarbonitrile (HOBC) bi-phase nematic liquid crystal composite films

Moliria V. Santos[a,*], Agnieszka Tercjak[b], Junkal Gutierrez[b], Hernane S. Barud[a,c], Mariana Napoli[a], Marcelo Nalin[a], Sidney J.L. Ribeiro[a]

[a] São Paulo State University (Unesp), Institute of Chemistry, CP 355, Araraquara, SP 14800-970, Brazil
[b] Group 'Materials + Technologies' (GMT), Department of Chemical and Environmental Engineering, Engineering College of Gipuzkoa, University of the Basque Country (UPV/EHU), Plaza Europa 1, 20018 Donostia-San Sebastián, Spain
[c] Laboratório de Biopolímeros e biomateriais (BioPolMat), Universidade de Araraquara, Araraquara, SP, Brazil

ARTICLE INFO

Article history:
Received 20 July 2016
Received in revised form 13 March 2017
Accepted 23 March 2017
Available online 27 March 2017

Keywords:
Bacterial cellulose nanocrystals
Iridescence films
Nematic liquid crystal
Thermo-responsive
Electro-responsive

ABSTRACT

The preparation of composite materials has gained tremendous attention due to the potential synergy of the combined materials. Here we fabricate novel thermal/electrical responsive photonic composite films combining cellulose nanocrystals (CNC) with a low molecular weight nematic liquid crystal (NLC), 4′-(hexyloxy)-4-biphenylcarbonitrile (HOBC). The obtained composite material combines both intense structural coloration of photonic cellulose and thermal and conductive properties of NLC. Scanning electron microscopy (SEM) results confirmed that liquid crystals coated CNC films maintain chiral nematic structure characteristic of CNC film and simultaneously, transversal cross-section scanning electron microscopy images indicated penetration of liquid crystals through the CNC layers. Investigated composite film maintain NLC optical properties being switchable as a function of temperature during heating/cooling cycles. The relationship between the morphology and thermoresponsive in the micro/nanostructured materials was investigated by using transmission optical microscopy (TOM). Conductive response of the composite films was proved by Electrostatic force microscopy (EFM) measurement. Designed thermo- and electro-responsive materials open novel simple pathway of fabrication of CNC-based materials with tunable properties.

1. Introduction

One recent international trend is to focus to develop novel cellulose nanocrystal-based materials with diverse advanced functionalities. Cellulose nanocrystals (CNC) may be prepared through controlled acid hydrolysis of bulk cellulose (Rånby, 1951). CNC are obtained as highly crystalline fibrils with nanometer dimensions and high-aspect-ratio rodlike that at sufficiently high concentrations in aqueous suspensions self-assemble in chiral nematic liquid crystalline phase (Revol, Bradford, Giasson, Marchessault, & Gray, 1992). The chiral nematic structure of CNC suspension can be preserved in solid films endowing the resulting materials with a helicoidal structure and brilliant iridescent colors (Revol, Godbout, & Gray, 1998). Integrating the optical properties of chiral nematic CNC structure with stimuli-responsive guest species may afford novel composites materials with an advanced set of functions, tunable properties and wide range of application possibilities. In this context, bio-derived photonic film formed by CNC have recently attracted attention as hosts for metal NPs (Chu et al., 2015; Qu et al., 2016; Querejeta-Fernandez et al., 2015), magnetic NPs (Espinha et al., 2016), shape memory polymers (Giese et al., 2016) and luminescent NPs (Chu et al., 2014).

In parallel, low molecular weight nematic liquid crystals (NLC) are organic macromolecules, that self-assembly depending on external stimuli such as electrical field, temperature and light (Doane, Vaz, Wu, & Žumer, 1986; Drzaic, 1986). These materials have been extensively used combined with polymers to design electro- and thermo-sensitive material where the dispersed mesophase can be switched from opaque scattering state (OFF-state) to transparent state (ON-state) due to matching of the refractive index of the polymer and that of the oriented NLC by applying an external electrical voltage or thermal gradi-

* Corresponding author.
E-mail address: moliriavs@iq.unesp.br (M.V. Santos).

http://dx.doi.org/10.1016/j.carbpol.2017.03.078
0144-8617/

ent (Campbell, Tasinkevych, & Smalyukh, 2014; Ganesan, Wirges, Mellinger, & Gerhard, 2010; Gutierrez, Tercjak, Algar, Retegi, & Mondragon, 2012; Tercjak & Gutierrez, 2011; Zhou, Collard, Park, & Srinivasarao, 2002). Also chiral nematic mesoporous silica have been combined with LCs to design thermal-optical devices (Giese et al., 2013; Manning et al., 2014).

Recently, some of us designed new optical materials by preparing composite films from NLC and bacterial cellulose (BC) self-sustainable membranes (Tercjak, Gutierrez, Barud, & Ribeiro, 2016). BC membranes display peculiar and unique properties that allow the utilization of this green material in different applications from biomedicine to photonics (Legnani et al., 2008; Pinto et al., 2015; Shah et al., 2013; Sulaeva, Henniges, Rosenau, & Potthast, 2015). Emergent properties of the composite materials so prepared include conductive and thermal response, characteristic of the coated NLC, added to thermal stability and mechanical properties of the BC membrane, for example. Therefore, the designed thermoresponsive materials displayed original tunable properties that would not be possible with the individual components (Tercjak et al., 2016).

Taking all these described features into account, the design of a new optical sensor platform is proposed here, that is, composite material based on CNC film and NLC. In contrast to examples mentioned above, where NLC were dispersed into the polymeric host, we proposed here a novel, facile and scalable approach based on the coating CNC film with NLC, resulting, upon evaporation, in iridescent films with thermal and conductive response.

CNC were extracted from BC membranes that were prepared at our laboratory as described before (Pinto et al., 2015; Tercjak et al., 2016). In the first step to obtain the new composites, iridescent CNC free-standing films around 40 μm thick were obtained by casting CNC suspensions on plastic substrates. In a second step CNC films were coated with the NCL 4′-(hexyloxy)-4-biphenylcarbonitrile (HOBC) by using the easy and inexpensive method proposed before (Tercjak et al., 2016). This new composite material was obtained as free-standing iridescent films, that exhibit tunable properties, in response to thermal gradient or relatively small electrical voltage in addition to the properties of the CNC films. The relationship between the surface structure and thermo-responsive properties of investigated HOBC coated CNC film was investigated using transmission optical microscopy (TOM). Additionally, electrostatic force microscopy (EFM) measurement was employed to prove the effect of external stimuli, in this case applied voltage, on the HOBC liquid crystal coated CNC film.

2. Materials and methods

2.1. Materials

Sulfuric acid (95–98%) was purchased from Sigma-Aldrich. Water was purified (Millipore Milli-Q purification system). Low molecular weight NLC, HOBC, was supplied by Sigma-Aldrich, and used without further purification. The thermal behavior of HOBC liquid crystal was evaluated by differential scanning calorimetry (DSC) (Fig. S1, Support information) and summarized in Scheme 1. HOBC displays crystalline-nematic transition at around 59 °C and nematic-isotropic transition around 76 °C.

2.1.1. Production of BC inoculum

The cellulose producing strain used was *Gluconacetobacter xylinus* (ATCC 23760) supplied by André Tosello Foundation, Campinas-SP, Brazil. It was cultured in Hestrim-Schramm medium (HS medium) that containing D-glucose glycose, yeast extract, peptone, di-sodium hydrogen phosphate (Na_2HPO_4), citric acid, agar and purified water. Analytical grade chemicals were used as received. Before the bacterial strain inoculation, the strain culture medium was sterilized and then was cultivated during 1 day at 28 °C in an air circulating oven as conditioning chamber.

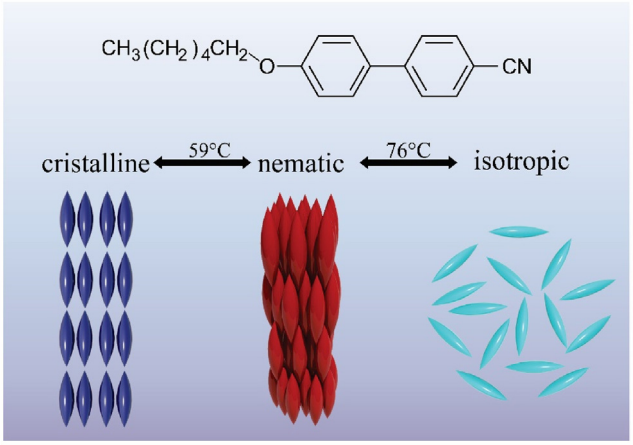

Scheme 1. HOBC Structure, crystal-nematic transition ($T_{C\text{-}N}$) and nematic-isotropic transition ($T_{N\text{-}I}$) obtained by DS.

2.1.2. Biosynthesis of BC

BC culture medium was prepared according to the method previously reported (dos Santos et al., 2014; Tercjak, Gutierrez, Barud, Domeneguetti, & Ribeiro, 2015). 45 mL of culture medium and 5 mL of the inoculum were cultivated during 3 days in static conditions at 28 °C in a 250 mL Erlenmeyer flask in an air circulating oven. After this time, jelly-like BC pellicle was harvested and purified to eliminate the culture medium (to remove the cells and other impurities). The purification protocol was realized following the pathway described before (Tercjak et al., 2015). Finally, purified BC hydrated membrane was dried in order to obtain BC film.

2.2. Preparation of CNC film

CNC were prepared according to the method previously reported (Dong, Revol, & Gray, 1998). Dried BC films (5 g) were milled using an IKA® A11 basic analytical mill and sieved with a stainless steel sieve (mesh 35) to ensure uniform particle size and to increase the surface area. The milled BC was hydrolyzed in 88 mL of a 64 wt% sulfuric acid solution at 50 °C for 0.5 h under vigorous stirring. The suspension was then diluted (10×) with ultrapure cold water (resistivity 18.2 MΩ cm at 25 °C) to stop the hydrolysis, and allowed to settle overnight. The clear top layer was decanted and the remaining cloudy layer was centrifuged at 6000 rpm for 10 min (Jouan C3i –CR3i multifunction centrifuge). The supernatant was decanted and the resulting thick white suspension was washed 3 times with ultrapure water. The thick white suspension was transferred to a dialysis cellulose membrane sleeve (12000–14000 molecular weight cut-off) and dialyzed against ultrapure water. The membrane sleeve containing the CNC were placed periodically in ultrapure water, and the procedure was continued until the pH of the water became constant (pH = 2.4) over a period of 1 h. The suspension was diluted to the desired concentration (3.0 wt%) and dispersed using an ultrasound homogenizer (Sonics Vibra-Cell VC 505 500W 20 kHz) with a 6 mm diameter probe. Typically, 50 mL of a 3.0 wt% CNC suspension was placed in a 100 mL plastic tube and sonicated at 60% of the maximum power (300 W). Prolonged sonication (to an energy input over 2500 J/g of CNC) was performed in an ice bath, to prevent desulfation caused by the heating generated during the process. Finally, 8 mL of CNC solution 3 wt% were transferred to polystyrene Petri dishes (diameter 45 mm), allowing

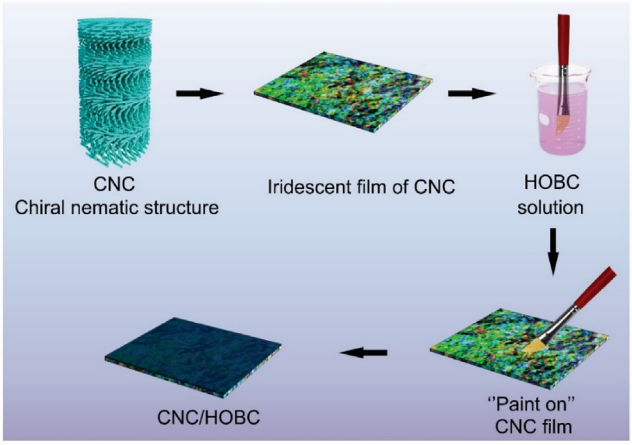

Scheme 2. Schematic diagram of the preparation method of the CNC/HOBC composite.

its evaporation at room temperature until free-standing films were formed.

2.3. Preparation of the composite film

Considering potential applications of designed materials, we have proposed an easy painting method, which can also be applied over large-scale areas at ambient conditions relatively inexpensively (Dunderdale, Urata, Miranda, & Hozumi, 2014; Tercjak et al., 2016). Thus, we fabricated CNC/HOBC films by the process illustrated in (Scheme 2). The CNC film was used as support for the HOBC coating. CNC film surface were painted with HOBC solution (3 wt% in chloroform) in order to get NLC coated CNC film.

2.4. Characterization of CNC and CNC/HOBC films

2.4.1. Thermal characterization

The thermal behavior of HOBC liquid crystal was analyzed on a Mettler Toledo DSC 822 differential scanning calorimeter equipped with a Sample Robot TSO 801 RO. Nitrogen was used as purge gas (10 mL min^{-1}). Temperature and enthalpy were calibrated by using an indium standard. Measurements were performed in sealed aluminum pans containing a sample weight of around 7 mg. The thermal behavior of the HOBC liquid crystal was analyzed from 0 °C to 150 °C with scan rate 10 °C min.

2.4.2. Morphological characterization

Morphological study of designed materials was performed using polarized optical microscopy (POM) and scanning electronic microscopy (SEM). The POM images were taken using an Olympus BX41 microscope, using the polarizers in a crossed arrangement. The SEM images were collected on a Hitachi SU-70 electron microscope. The samples were attached to aluminum stubs using double-sided carbon adhesive tape or carbon glue. The images were taken from the surface and the cross-section areas. All the samples were sputter-coated with carbon with an EMITECH K950X Turbo Evaporator using a single pulse, outgassing time of 30 s and evaporating time of 2 s.

2.4.3. Structural characterization

CNC and CNC/HOBC films were structurally characterized by ATR Fourier transform infrared spectroscopy carried out using a Nicolet Nexus Spectra equipped with a Golden Gate single reflection diamond ATR accessory. The ATR-FTIR spectra of CNC and CNC/HOBC films were taken with a 2 cm^{-1} resolution in a wavenumber range from 4000 to 400 cm^{-1}.

2.4.4. Optical characterization

Emission spectra were recorded at room temperature with a modular double grating excitation spectrofluorimeter with a TRIAX 320 emission monochromator (Fluorolog-3, Horiba Scientific) coupled to a R928 Hamamatsu photomultiplier, using a front face acquisition mode. The excitation source was a 450 W Xe arc lamp. UV–vis spectroscopy was carried out using a Perkin-Elmer lambda 950 UV/Vis/NIR spectrophotometer and Spectralon integrating sphere (ϕ = 150 mm). The freestanding films surface was placed perpendicular to the incidence beam and the spectra were acquired as function of the angle ($20° < \theta < 70°$).

The effect of temperature on the properties of the investigated films was verified in situ by UV–vis spectroscopy using a Cary 5000 UV–vis spectrometer (Varian), in the range of energy from 1500 to 200 nm, coupled to an oven working in the temperature range from 20 to 80 °C with the rate 1 °C/min.

2.4.5. Thermo-responsive properties

Thermo-responsive properties of CNC/HOBC film were studied by TOM under cross-polarized light carried out using a Nikon Eclipse E600W microscope equipped with a hot stage Mettler FP 82 HT. Samples were exposed to a heating/cooling process from 30 °C to 70 °C at 2 °C/min and the images were captured in both processes.

2.4.6. Conductive properties

Atomic force microscopy (AFM) measurement was performed using a Dimension Icon scanning probe microscope equipped with Nanoscope V controller (Bruker). Tapping mode (TM) was employed in air using an integrated tip/cantilever (125 μm in length with ca. 300 kHz resonant frequency). Typical scan rates during recording were 0.9–1.1 line/s using a hybrid scan head with a maximum range of 100 × 100 μm. EFM was used to study the conductive properties of liquid crystals coated CNC film. Measurements were performed using the same scanning probe microscopy (Nanoscope V, Dimension ICON from Bruker) operating in the Lift-Mode (lift height was ~120–150 nm) in ambient conditions and equipped with a Pt/Ir coating tip with a resonance frequency around 75 kHz. The secondary imaging mode derived from tapping mode that measures electric field gradient distribution above the sample surface has been detected by applying a voltage to the cantilever tip. Locally charged LC phase domains on the samples surface were qualitatively mapped simultaneously with the height and phase AFM images. Different regions of the samples were scanned to ensure that both morphology and conductive properties of the investigated materials are the representative one.

3. Results

3.1. Morphological characterization

POM images of CNC film (Fig. 1a) show pronounced iridescence under unpolarized room light. The first order Bragg reflection is observed (Lagerwall et al., 2014). In selected regions of the sample, fingerprint lines, characteristic of chiral nematic regions viewed orthogonal to the chiral nematic axis, are in focus (Fig. 1b). The images (Fig. 1a and b) display a mosaic of domains with different shapes and colors such as green, blue and orange due to anisotropy of CNC films. Pitch lengths and helicoid tilt axes are different in different regions, reflecting light with much wider bandwidth than single-pitch CNC films (Steiner & Vignolini, 2014). Similarly, POM images of CNC/HOBC composite exhibit iridescence under unpo-

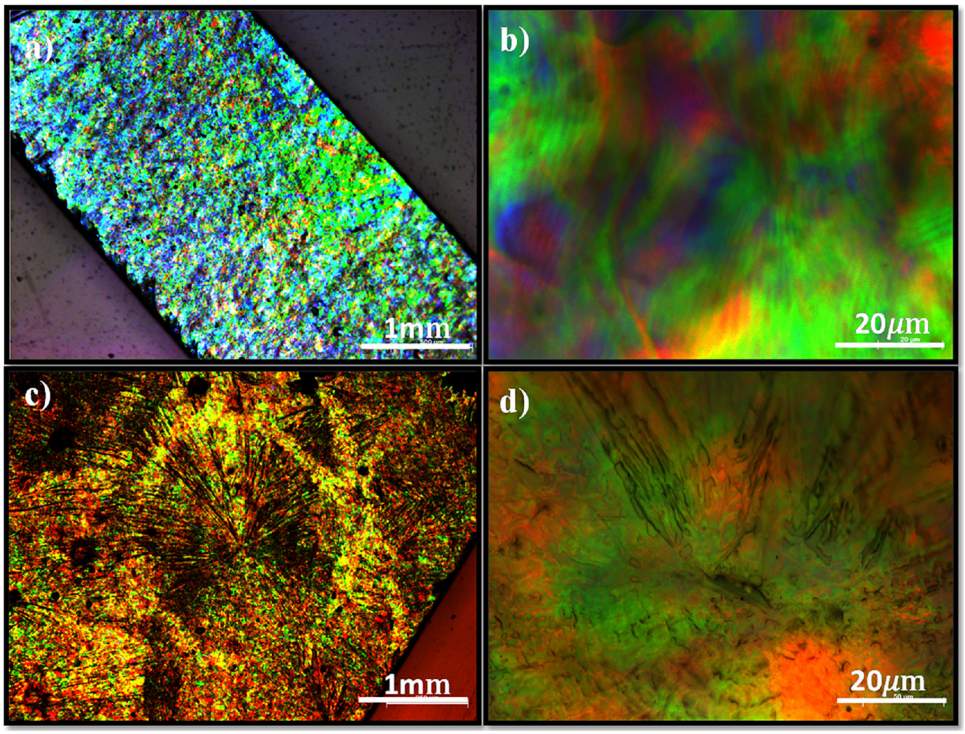

Fig. 1. (a and b) POM images of iridescent film of CNC showing a fingerprint texture characteristic of chiral nematic ordering. (c and d) POM image of CNC/HOBC displays formation of spherulites of HOBC covering a larger area of the CNC surface.

larized room light (Fig. 1c) indicating that the chiral nematic phase was retained after LC coating (Fig. 1b). However, the domains with different orientations are not visible. Spherulitic crystallization of HOBC covered surface of CNC film is observed instead (Tercjak, Serrano, Larrañaga, & Mondragon, 2008).

SEM provided further confirmation of the chiral nematic organization into the CNC films that was preserved after drying (Fig. 2). The SEM image of the surface film (Fig. 2a) shows aligned cellulose nanocrystals. The edge view of a cracked film (Fig. 2b) shows the long-range layered structure with twisted spindle-like features rotated in a counter-clockwise direction, indicating the nanocrystals form a left-handed helicoids (Majoinen, Kontturi, Ikkala, & Gray, 2012). The cross-section of the CNC film is shown in Fig. 2c, the micrograph shows the film thickness around 40.8 μm. At higher magnification (Fig. 2d) one distinguishes the periodic structure formed by regularly spaced layers achieved due to self-assembly of the nanocrystallites, where each repeating band corresponds to a 180° rotation of the chiral nematic director (a half helical pitch) (Ping et al., 2013; Steiner & Vignolini, 2014) . Deeper analysis of Fig. 2d, allowed to conclude that the regularly spacing corresponds to a pitch value of 118 ± 12 nm.

SEM image of CNC/HOBC film (Fig. 3a) shows the NLC coating on the cellulose nanocrystals of the CNC film. The cross-section micrographs are shown in Fig. 3c and d. Thickness of composite film was observed to increase from about 40.8 μm for initial CNC film (Fig. 2d) to around 60.2 μm (Fig. 3b). The increasing thickness can be related not only to coating HOBC liquid crystals, but also to the swelling of the CNC film as result of penetration of part of the HOBC liquid crystals through the multilayered structure of cellulose nanocrystals of CNC film. Interesting enough, the edge micrograph of the cracked film (Fig. 3b) and the higher magnification of cross-section show that the chiral nematic phase was retained in the CNC film after NLC coating. Moreover, the higher magnification image (Fig. 3d) exhibits the fingerprint lines throughout their entire thickness. The periodic structure observed in CNC film was preserved and regularly spacing corresponds to a pitch value of 118 ± 12 nm.

3.2. Structural characterization

Fig. S2 (Supporting Information) shows ATR-FTIR spectra. The spectrum obtained for CNC film showed characteristics bands of cellulose at 3345 cm^{-1} (ν O—H of cellulose type I), 3240 cm^{-1} (hydrogen bond O—H), 2895 cm^{-1} (ν C—H of CH_2 groups), 2854 cm^{-1} (ν_{as} CH_2), 1650 cm^{-1} (bending motion of absorbed water, δ H—O—H), 1426 cm^{-1} (δ_s CH_2), 1365 cm^{-1} (δ C—H), 1160 cm^{-1} (ν_{as} C—O—C), and 1060 cm^{-1} (ν C—O) (Barud et al., 2008; Kondo & Sawatari, 1996; Oh et al., 2005).

The spectrum obtained for HOBC displayed bands at 1098 cm^{-1} (ν C—O—C group of the ether bond), 1458 cm^{-1} (δ C—H), 1594 cm^{-1} (axial δ of C=C of the aromatic ring), 2355 and 2211 cm^{-1} (axial δ of C ≡N) and 2855 e 2915 cm^{-1} (ν C—H of CH_2 and CH_3 groups).

Spectra obtained for CNC/HOBC composites display bands observed for the two components of the composites. The decreasing relative intensity of the —OH stretching bands relates to the NCL coating on CNC film, as observed by SEM measurements (Fig. 3a). Supporting this result the intensity of the ν C—H vibration of CH_2 and CH_3 groups was higher in the spectrum obtained for the composite film. Additional characteristic HOBC peaks are observed at 1458 cm^{-1} (δ C—H), 1594 cm^{-1} (axial δ of C=C of the aromatic ring) and 2211 cm^{-1} (axial δ of C ≡N).

No further new band, relative intensities change or band shift, that could be a signature of chemical interactions between the two counterparts, were observed.

Nematic HOBC liquid crystals show photoluminescence (PL) properties (Tercjak, Gutierrez, Ocando, Peponi, & Mondragon, 2009). The PL spectra of pristine HOBC and CNC/HOBC composite are shown in Fig. S3 (Supporting information). The broad emission band observed for CNC/HOBC composite appears almost in the same range as the emission band of the pristine HOBC with

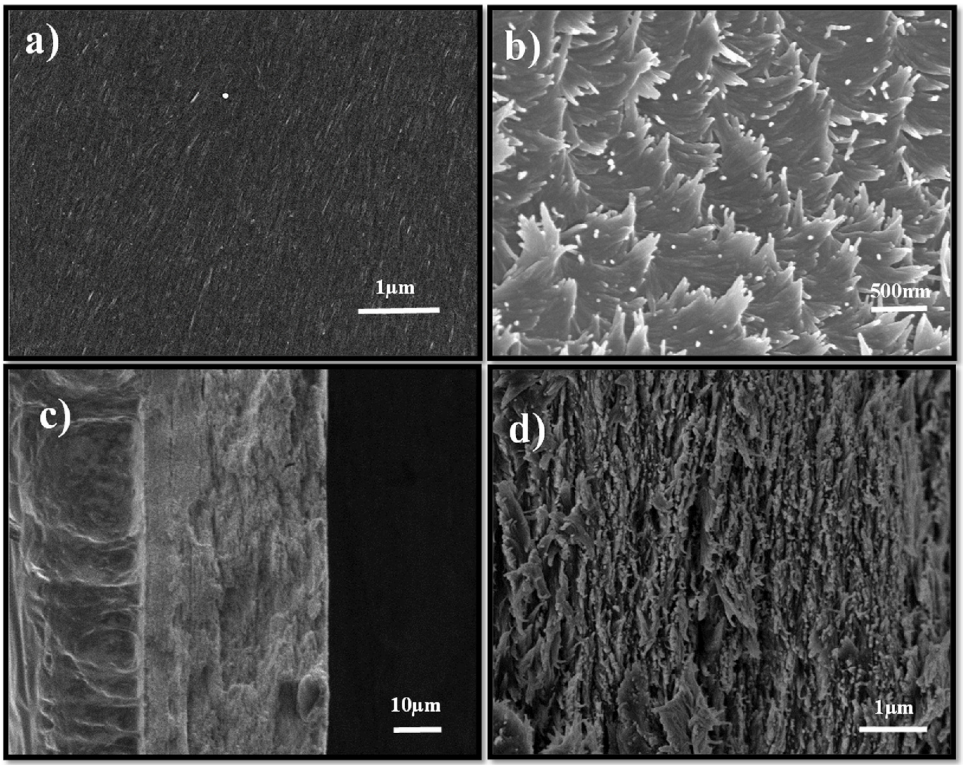

Fig. 2. SEM images of CNC film: (a) SEM image of film surface formed by aligned nanocrystals cellulose; (b) Side view of a cracked film showing the layered structure of the nanocrystals and the rod-like morphology with the rods twisted in a left-handed orientation; (c) Image of fracture surface across the CNC film; (d) Higher magnification side view of fracture surface across the CNC film shows the stacked layers that result from the helical pitch of the chiral nematic phase.

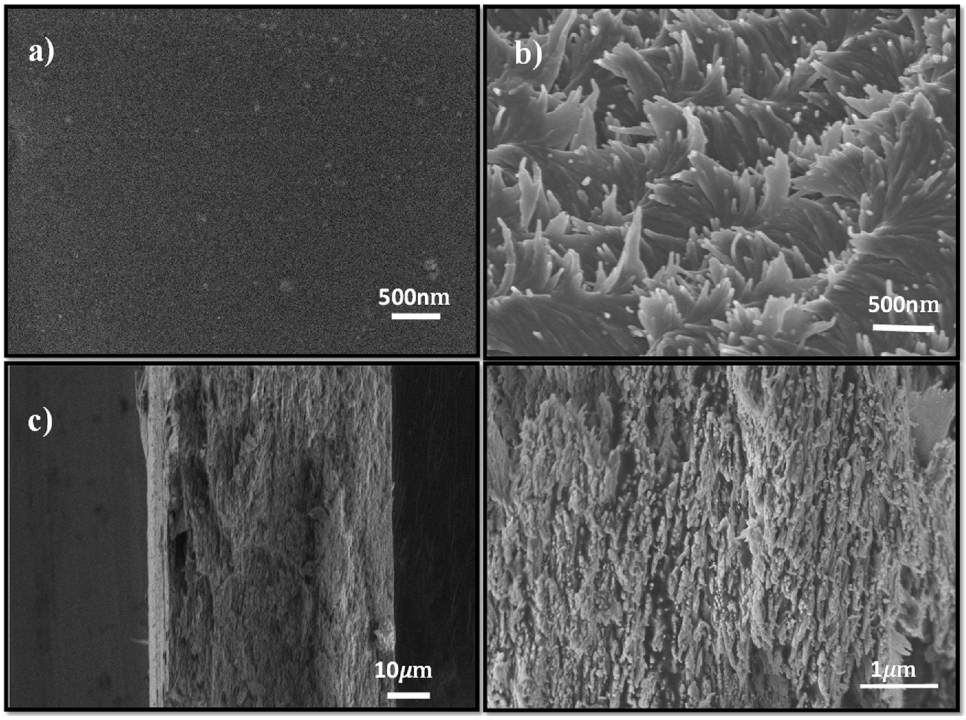

Fig. 3. SEM images of CNC/HOBC composite: (a) Image of film surface of CNC covered by the liquid crystal HOBC; (b) Side view of a cracked film shows the layered structure of the nanocrystals and the rod-like morphology with the rods twisting in a left-handed orientation; (c) Image of cross section of fracture film (thickness 60.2 μm); (d) The magnification of the side view of the fractured surface across film, shows the layered structure of the nanocrystals.

the maximum intensity around 345 nm. These results confirm the effective way of addition of low molecular weight HOBC liquid crystals coating CNC film, with preserved properties.

3.3. Optical characterization

Fig. 4 shows transmission spectra obtained at normal incident angle ($\theta = 0^\circ$). Bragg diffraction peaks are observed with a characteristic maximum wavelength (λ_0), in the visible part of the spectra at around 500 nm. Spectra obtained for CNC/HOBC composites show an additional absorption band of the liquid crystal at around 290 nm, which refers to molecular electronic transition $\pi \rightarrow \pi^*$ of HOBC molecules. These results also suggest of effective addition of low molecular weight HOBC liquid crystals coating CNC film. In addition, these results demonstrated that the HOBC coating do not affect in the optical properties of CNC film, contrary what it has been observed in the literature, in which even the ambient humidity and water content of the films can affects the film properties (Niinivaara, Faustini, Tammelin, & Kontturi, 2016; Niinivaara, Faustini, Tammelin, & Kontturi, 2015).

Fig. S4a (Supporting Information) shows reflectance spectra obtained as function of the incident angle ($15^\circ < \theta < 60^\circ$). Bragg diffraction is confirmed by the variation of the peak position as function of incident angle (θ). The peak maximum wavelength (λ_0) obeys the Vries' relationship (Eq. (1)) where the reflection peak shifts to shorter wavelengths as the viewing angle increases relative to the normal of the film.

$$\lambda_0 = n_{ave} P \cos\theta \quad (1)$$

(θ) is the incident angle between the surface normal and the incident ray, P is pitch of chiral nematic structure, and n_{ave} is the average refractive indice. Using De Vries equation and λ_0 the pitch of the chiral nematic structure P may be determined as shown in Fig. S4b (Supporting Information). The P calculated is 119 ± 4 nm for CNC/HOBC, this value is comparable with P obtained from SEM measurements.

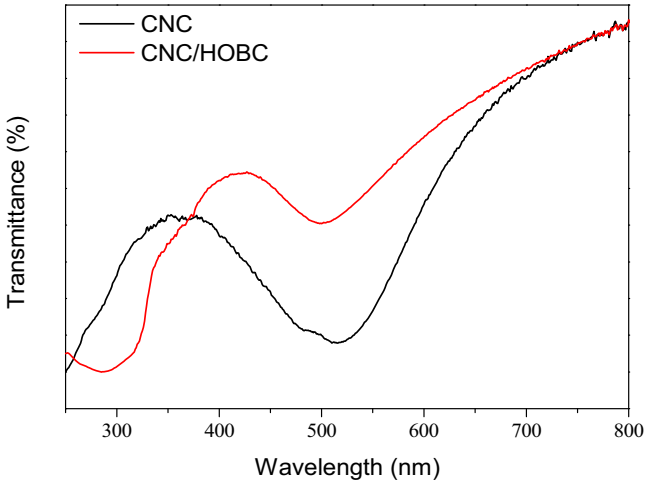

Fig. 4. Transmission spectra of the films CNC and CNC/HOBC.

Thermo-optical properties of CNC/HOBC composites were also studied by UV–vis transmittance spectroscopy as function of the temperature. Fig. 5a shows spectra obtained for pristine HOBC deposited on a quartz substrate. The opaque (OFF state) to transparent (ON state) transition is well known to be observed in the 56–60 °C range (Tercjak, Garcia, & Mondragon, 2008; Tercjak et al., 2009; Tercjak & Gutierrez, 2011; Tercjak, Gutierrez, Ocando, & Mondragon, 2010). Fig. 5b also shows spectra obtained for the composites. The OFF-ON transition is well observed superposed to the stop-band of photonic structure of CNC/HOBC film. Therefore, liquid crystalline properties from both NLC coating and CNC film substrate are well preserved in the new materials prepared. In previous work using BC membranes as substrates, the NLC properties were also preserved in BC-NLC composites. Interesting enough here we present results where the substrate present liquid crystalline organization as well combining the optical properties of CNC film and the thermal behavior of NLC. These results open novel sim-

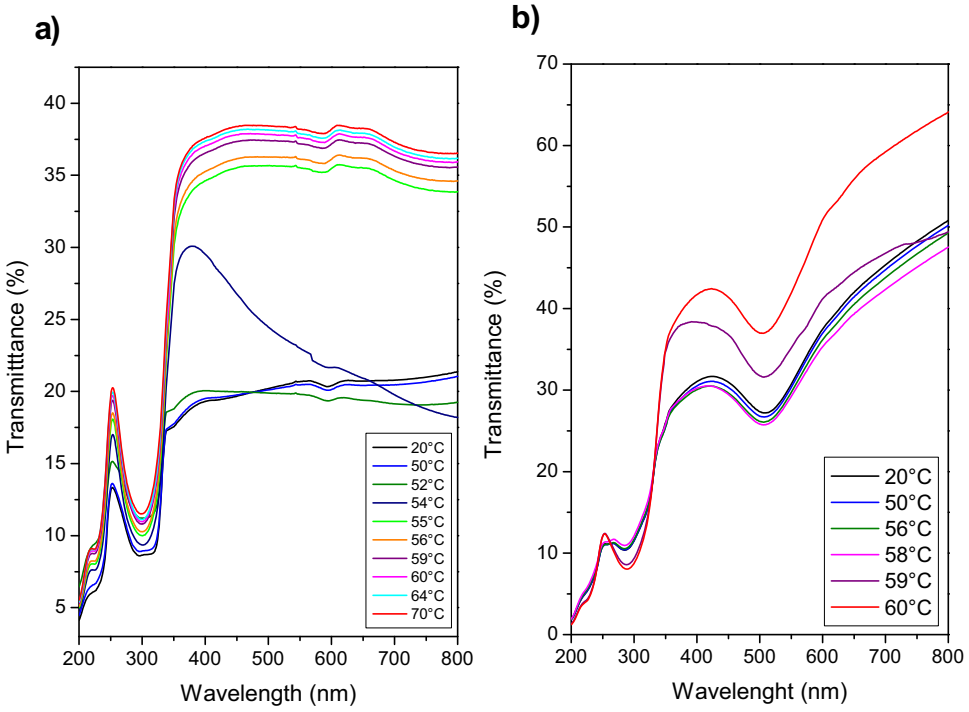

Fig. 5. Transmission spectra as function of the temperature: (a) HOBC; (b) CNC/HOCB.

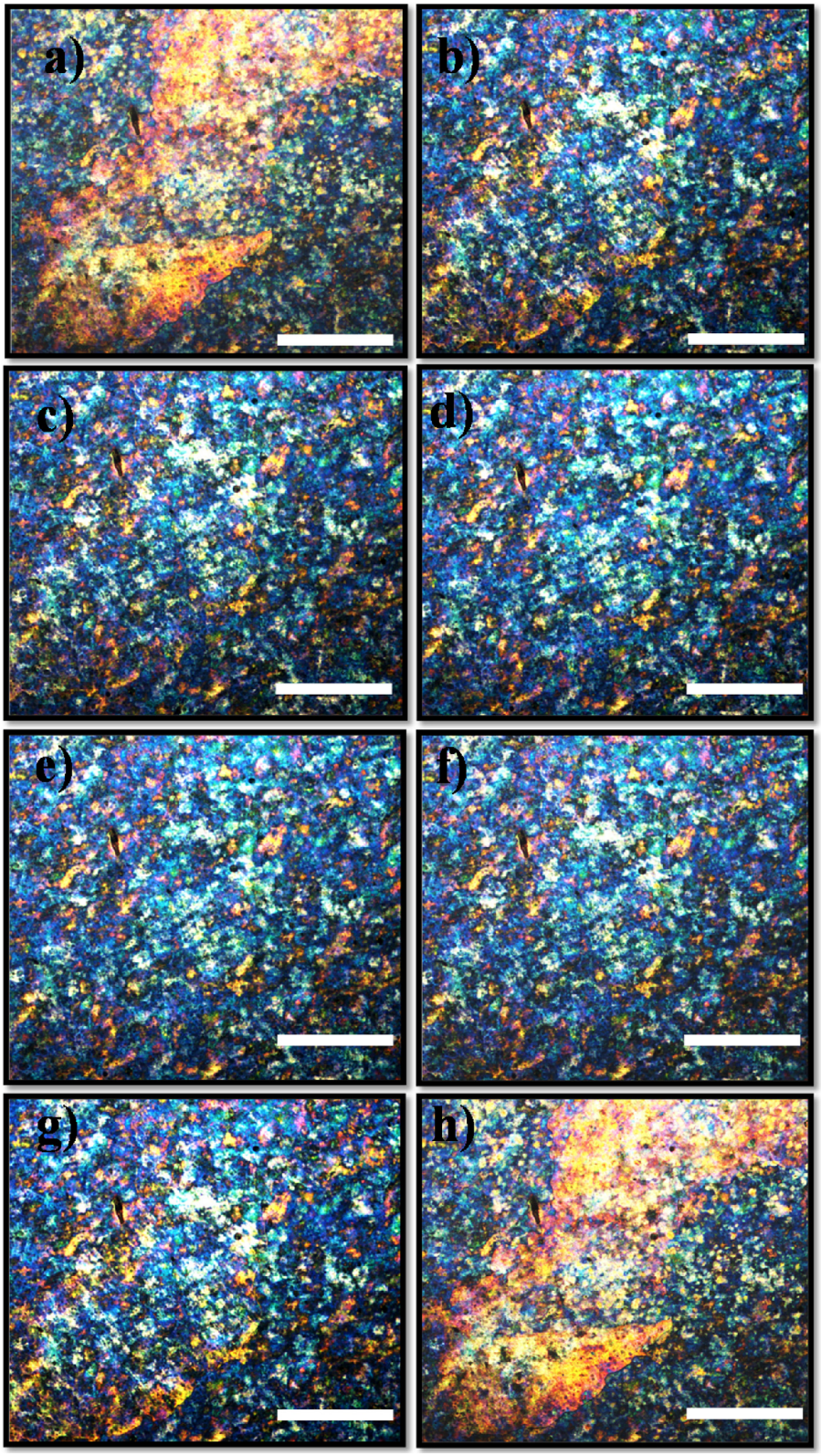

Fig. 6. TOM micrographs of CNC/HOBC during heating taken at: (a) 30 °C (b) 47 °C, (c) 56 °C, (d) 60 °C and during cooling at: (e) 60 °C (f) 55 °C (g) 45 °C (h) 30 °C. (scale bar, 200 μm).

ple pathway of fabrication of CNC-based materials with tunable properties.

Thermo-responsive properties of CNC/HOBC composite were also investigated by transmission optical microscopy in heating/cooling processes under cross-polarized light using hot stage mode. Representative TOM micrographs taken during heating and cooling process are shown in Fig. 6. The melting transition of HOBC phase of CNC/HOBC composite took place at around 47 °C. Similarly, to the thermo-reversible behavior observed by UV–vis measurement, the range of switching between opaque and transparent

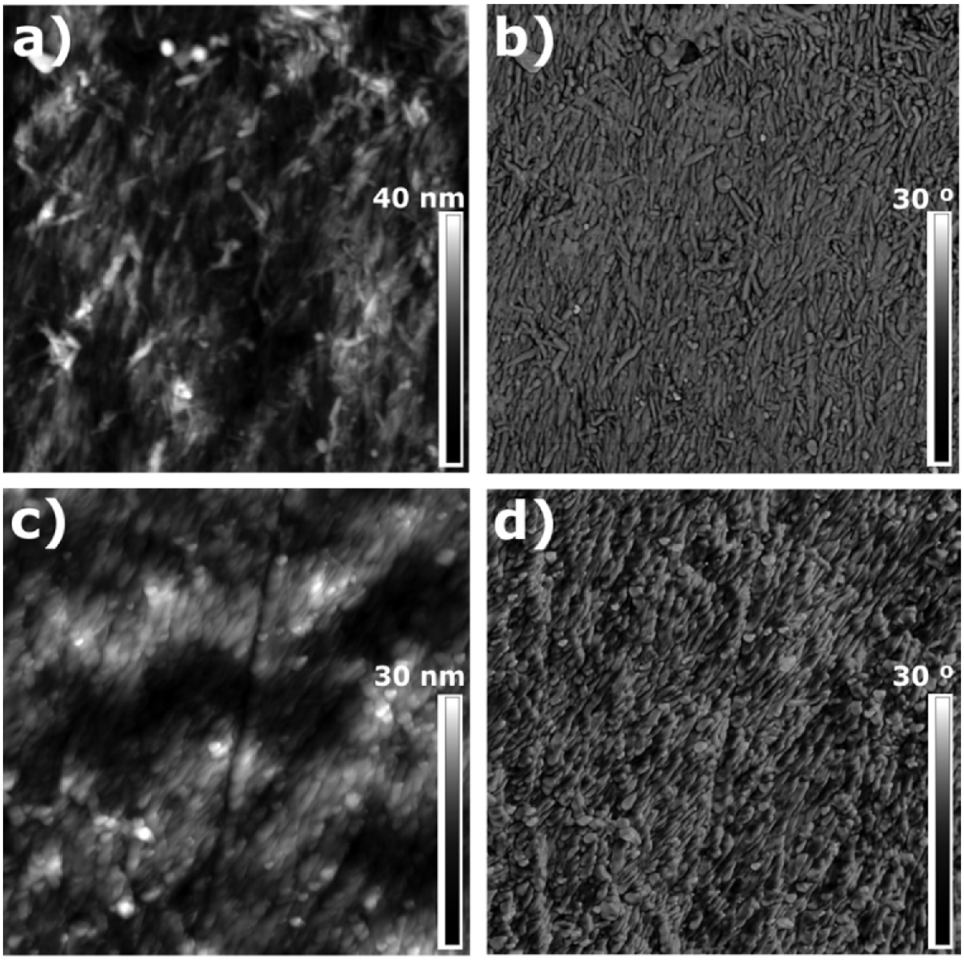

Fig. 7. TM-AFM (3 μm × 3 μm) height (a) and phase (b) images of CNC and TM-AFM height (a) and phase (b) images of CNC/HOBC film.

state of NLC during cooling/heating cycle was narrower and switching took place almost in the same temperature in both cooling and heating processes, being at the temperature range 56–60 °C for heating process and 55–60 °C for the cooling process. Thermoreversible behavior of CNC/HOBC composite also confirmed that pristine HOBC transfer their properties to the investigated composite.

TM-AFM height and phase images are shown in Fig. 7. Results obtained for the CNC film confirmed orientation of nanocrystals as already observed by SEM results. Similar results have been reported by Usov and co-wokers investigate different types of nanocelluloses (Usov et al., 2015). Moreover, using AFM one could easily distinguish individual nanocrystals composing the CNC film. The regular size of homogeneously distributed nanocrystals was 25 ± 5 nm in diameter and 200 ± 20 nm in length (Fig. 7b). Comparing results obtained for CNC and CNC/HOBC films, it observed liquid crystal coating on cellulose nanocrystals surface lead to smoother surface which confirmed the TM-AFM height images (40 nm for CNC film and 30 nm for HOBC coated CNC film). This behavior was verified with decrease of the average roughness (Ra), extracted from TM-AFM height images, from 5 nm to 4 nm for CNC and CNC/HOBC films, respectively.

Electrostatic force microscopy was employed to verify transfer of the conductive response of the HOBC liquid crystal to composites. Fig. 8 shows AFM phase and EFM phase images, taken simultaneously, scanned applying 0, 6, −6 V. As expected, any charged domains were detected at the surface of HOBC coated CNC film when 0 V was applied to the EFM-tip (Fig. 8b). On the contrary, as seen in Fig. 8c and d, by applying 6 and −6 V to the EFM-tip allowed to distinguish charged domains confirming that HOBC coated CNC film respond on the applied voltage independently on the sign (positive or negative) of the voltage values. Applying both 6 and −6 V one can easily detect charged domains well distributed on the whole investigated surface mapped with low contrast level of the EFM phase image around 3°. Low contrast ensures weak response on the applied voltage corresponding to electrostatic force between the sample and EFM-tip. Here it should be pointed out that CNC film did not show any charged domains, when 6 and −6 V were applied to the EFM-tip indicating that HOBC liquid crystal transfer its ability to respond on the external stimuli (applied voltage) to the fabricated HOBC coated CNC film.

4. Conclusion

By using cellulose nanocrystals (CNC) films and 4′-(hexyloxy)-4-biphenylcarbonitrile (HOBC) novel multifunctional composite films were obtained. The new material integrates iridescence, conductive and thermal response. The designed materials were obtained as free-standing films with chiral nematic organization. The cross-section SEM images confirmed HOBC liquid crystals covering the surface of CNC films and also present in between of multilayered structure of cellulose nanocrystals of CNC film. The thermo-optical properties were evaluated by UV–vis transmittance spectroscopy as function of the temperature, with brush

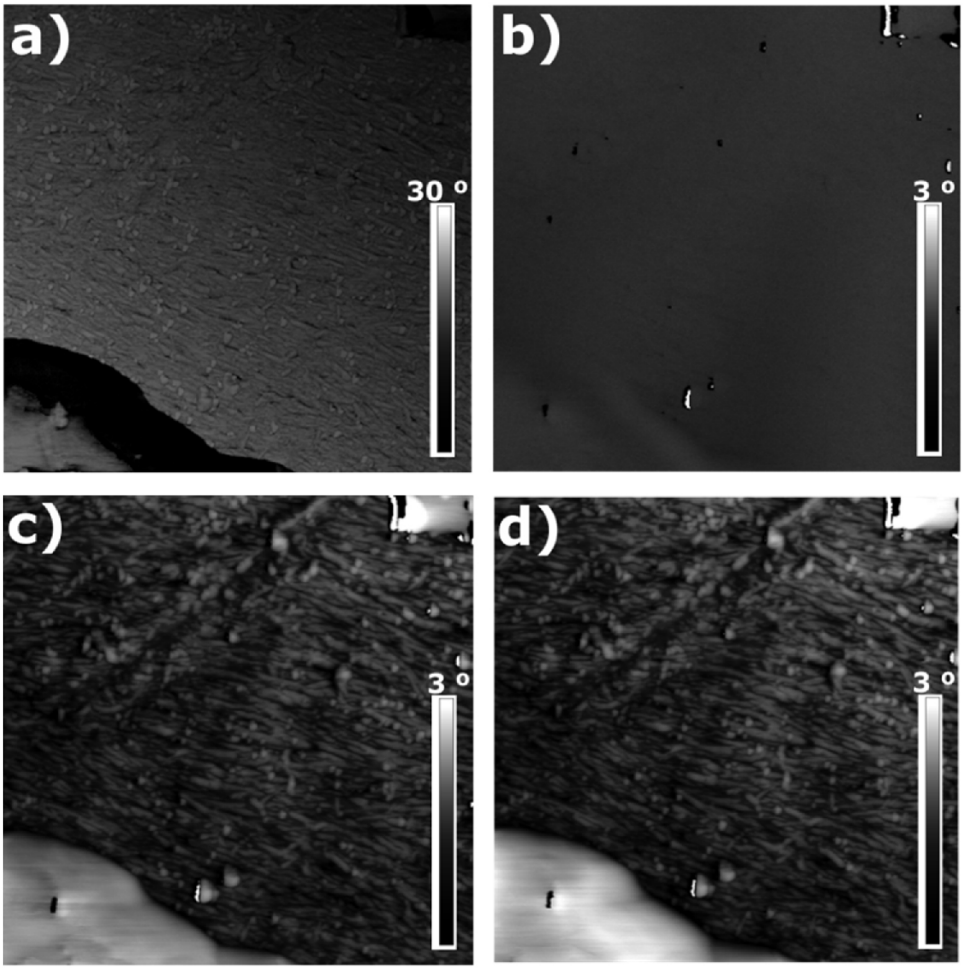

Fig. 8. (a) AFM phase image (3 μm × 3 μm) and EFM phase images (3 μm × 3 μm) of CNC/HOBC film obtained applying (b) 0 V, (c) 6 V and (d) −6 V.

surfaces possessing modulated optical properties as response to temperature. Additionally, EFM measurement confirmed conductive response of the brush surfacesas response to the voltage applied to the AFM tip. Therefore a novel strategy to design cellulose nanocrystal based materials with thermoresponsive and conductive properties, keeping optical properties of CNC film, was developed. The composites presented attractive properties to the development in the field of thermo- and electro optical devices, such as smart windows, optical sensors and display devices.

Author contributions

The manuscript was written through contributions of all authors. All authors have given approval to the final version of the manuscript.

Notes

The authors declare no competing financial interest.

Acknowledgments

This work was supported by Brazilian agencies São Paulo Research Foundation, grants #2014/12424-2, #2012/05087-4 and #2013/07793-6, CNPq and CAPES. Moreover, we are grateful to the Macrobehavior-Mesostructure-Nanotechnology unit of the UPV/EHU.

Appendix A. Supplementary data

Supplementary data associated with this article can be found, in the online version, at http://dx.doi.org/10.1016/j.carbpol.2017.03.078.

References

Barud, H. S., Assunção, R. M. N., Martines, M. A. U., Dexpert-Ghys, J., Marques, R. F. C., Messaddeq, Y., & Ribeiro, S. J. L. (2008). Bacterial cellulose–silica organic–inorganic hybrids. *Journal of Sol-Gel Science and Technology*, *46*(3), 363–367.

Campbell, M. G., Tasinkevych, M., & Smalyukh, I. I. (2014). Topological polymer dispersed liquid crystals with bulk nematic defect lines pinned to handlebody surfaces. *Physical Review Letters*, *112*(19), 19780.

Chu, G., Xu, W., Qu, D., Wang, Y., Song, H., & Xu, Y. (2014). Chiral nematic mesoporous films of Y_2O_3: Eu^{3+} with tunable optical properties and modulated photoluminescence. *Journal of Materials Chemistry C*, *2*(43), 9189–9195.

Chu, G., Wang, X., Chen, T., Xu, W., Wang, Y., Song, H., & Xu, Y. (2015). Chiral electronic transitions of YVO_4: Eu^{3+} nanoparticles in cellulose based photonic materials with circularly polarized excitation. *Journal of Materials Chemistry C*, *3*(14), 3384–3390.

Doane, J. W., Vaz, N. A., Wu, B., & Žumer, S. (1986). Field controlled light scattering from nematic microdroplets. *Applied Physics Letters*, *48*(4), 269–271.

Dong, X. M., Revol, J. F., & Gray, D. G. (1998). Effect of microcrystallite preparation conditions on the formation of colloid crystals of cellulose. *Cellulose*, *5*(1), 19–32.

Drzaic, P. S. (1986). Polymer dispersed nematic liquid crystal for large area displays and light valves. *Journal of Applied Physics*, *60*(6), 2142–2148.

Dunderdale, G. J., Urata, C., Miranda, D. F., & Hozumi, A. (2014). Large-scale and environmentally friendly synthesis of pH-responsive oil-repellent polymer brush surfaces under ambient conditions. *ACS Applied Materials and Interfaces*, *6*(15), 11864–11868.

Espinha, A., Guidetti, G., Serrano, M. C., Frka-Petesic, B., Dumanli, A. G., Hamad, W. Y., . . . & Vignolini, S. (2016). Shape memory cellulose-based photonic reflectors. *ACS Applied Materials and Interfaces*, *8*(46), 31935–31940.

Ganesan, L. M., Wirges, W., Mellinger, A., & Gerhard, R. (2010). Piezo-optical and electro-optical behaviour of nematic liquid crystals dispersed in a ferroelectric copolymer matrix. *Journal of Physics D: Applied Physics*, *43*(1), 15401.

Giese, M., De Witt, J. C., Shopsowitz, K. E., Manning, A. P., Dong, R. Y., Michal, C., . . . & Maclachlan, M. J. (2013). Thermal switching of the reflection in chiral nematic mesoporous organosilica films infiltrated with liquid crystals. *ACS Applied Materials and Interfaces*, *5*, 6854–6859.

Giese, M., Blusch, L. K., Schlesinger, M., Meseck, G. R., Hamad, W. Y., Arjmand, M., & MacLachlan, M. J. (2016). Magnetic mesoporous photonic cellulose films. *Langmuir*, *32*(36), 9329–9334.

Gutierrez, J., Tercjak, A., Algar, I., Retegi, A., & Mondragon, I. (2012). Conductive properties of TiO2/bacterial cellulose hybrid fibres. *Journal of Colloid And Interface Science*, *377*(1), 88–93.

Kondo, T., & Sawatari, C. (1996). A fourier transform infra-red spectroscopic analysis of the character of hydrogen bonds in amorphous cellulose. *Polymer*, *37*(3), 393–399.

Lagerwall, J. P. F., Schütz, C., Salajkova, M., Noh, J., Hyun Park, J., Scalia, G., & Bergström, L. (2014). Cellulose nanocrystal-based materials: From liquid crystal self-assembly and glass formation to multifunctional thin films. *NPG Asia Materials*, *6*(1)

Legnani, C., Vilani, C., Calil, V. L., Barud, H. S., Quirino, W. G., Achete, C. A., . . . & Cremona, M. (2008). Bacterial cellulose membrane as flexible substrate for organic light emitting devices. *Thin Solid Films*, *517*(3), 1016–1020.

Majoinen, J., Kontturi, E., Ikkala, O., & Gray, D. G. (2012). SEM imaging of chiral nematic films cast from cellulose nanocrystal suspensions. *Cellulose*, *19*(5), 1599–1605.

Manning, A. P., Giese, M., Terpstra, A. S., MacLachlan, M. J., Hamad, W. Y., Dong, R. Y., & Michal, C. A. (2014). NMR of guest-host systems: 8CB in chiral nematic porous glasses. *Magnetic Resonance in Chemistry*, *52*(10), 532–539.

Niinivaara, E., Faustini, M., Tammelin, T., & Kontturi, E. (2015). Water vapor uptake of ultrathin films of biologically derived nanocrystals: quantitative assessment with quartz crystal microbalance and spectroscopic ellipsometry. *Langmuir*, *31*(44), 12170–12176.

Niinivaara, E., Faustini, M., Tammelin, T., & Kontturi, E. (2016). Mimicking the humidity response of the plant cell wall by using two-dimensional systems: The critical role of amorphous and crystalline polysaccharides. *Langmuir*, *32*(8), 2032–2040.

Oh, S. Y., Dong, I. Y., Shin, Y., Hwan, C. K., Hak, Y. K., Yong, S. C., . . . & Ji, H. Y. (2005). Crystalline structure analysis of cellulose treated with sodium hydroxide and carbon dioxide by means of X-ray diffraction and FTIR spectroscopy. *Carbohydrate Research*, *340*(15), 2376–2391.

Ping, Y., Chodavarapu, V. P., Kirk, A. G., & Andrews, M. P. (2013). Sensors and Actuators B: Chemical Structured color humidity indicator from reversible pitch tuning in self-assembled nanocrystalline cellulose films. *Sensors & Actuators: B. Chemical*, *176*, 692–697.

Pinto, E. R. P., Barud, H. S., Silva, R. R., Palmieri, M., Polito, W. L., Calil, V. L., . . . & Messaddeq, Y. (2015). Transparent composites prepared from bacterial cellulose and castor oil based polyurethane as substrates for flexible OLEDs. *Journal of Materials Chemistry C*, *3*(44), 11581–11588.

Qu, D., Zhang, J., Chu, G., Jiang, H., Wu, C., & Xu, Y. (2016). Chiral fluorescent films of gold nanoclusters and photonic cellulose with modulated fluorescence emission. *Journal of Materials Chemistry C*, *4*(9), 1764–1768.

Querejeta-Fernandez, A., Kopera, B., Prado, K. S., Klinkova, A., Methot, M., Chauve, G., . . . & Kumacheva, E. (2015). Circular dichroism of chiral nematic films of cellulose nanocrystals loaded with plasmonic nanoparticles. *ACS Nano*, *9*(10), 10377–10385.

Rånby, B. G. (1951). Fibrous macromolecular systems. Cellulose and muscle. The colloidal properties of cellulose micelles. *Discussions of the Faraday Society*, *11*, 158–164.

Revol, J.-F., Bradford, H., Giasson, J., Marchessault, R. H., & Gray, D. (1992). Helicoidal self-ordering of cellulose microfibrils in aqueous suspension. *International Journal of Biological Macromolecules*, *14*, 170–172.

Revol, J.-F., Godbout, L., & Gray, D. G. (1998). Solid self-assembled films of cellulose with chiral nematic order and optically variable properties. *Journal of Pulp and Paper Science*, *24*(5), 146–149.

Shah, N., Ul-Islam, M., Khattak, W. A., & Park, J. K. (2013). Overview of bacterial cellulose composites: A multipurpose advanced material. *Carbohydrate Polymers*, *98*(2), 1585–1598.

Steiner, U., & Vignolini, S. (2014). Digital color in cellulose nanocrystal films. *ACS Applied Materials & Interfaces*, *6*(15), 12302–12306.

Sulaeva, I., Henniges, U., Rosenau, T., & Potthast, A. (2015). Bacterial cellulose as a material for wound treatment: Properties and modifications. A Review. *Biotechnology Advances*, *33*(8), 1547–1571.

Tercjak, A., & Gutierrez, J. (2011). Conductive properties of photoluminescent Au/Ps-b-PEO inorganic/organic hybrids containing nematic liquid crystals. *The Journal of Physical Chemistry C*, *115*(5), 1643–1648.

Tercjak, A., Garcia, I., & Mondragon, I. (2008). Liquid crystal alignment in electro-responsive nanostructured thermosetting materials based on block copolymer dispersed liquid crystal. *Nanotechnology*, *19*(27), 275701.

Tercjak, A., Serrano, E., Larrañaga, M., & Mondragon, I. (2008). Polymer dispersed liquid crystals based on poly(styrene-b-ethylene oxide), poly(bisphenol a carbonate) or poly(methylphenylsiloxane), and 4′-(hexyloxy)-4-biphenyl-carbonitrile: Analysis of phase diagrams and morphologies generated. *Journal of Applied Polymer Science*, *108*(2), 1116–1125.

Tercjak, A., Gutierrez, J., Ocando, C. J., Peponi, L., & Mondragon, I. (2009). Thermoresponsive inorganic/organic hybrids based on conductive TiO_2 nanoparticles embedded in poly (styrene-b-ethylene oxide) block copolymer dispersed liquid crystals. *Acta Materialia*, *57*(15), 4624–4631.

Tercjak, A., Gutierrez, J., Ocando, C., & Mondragon, I. (2010). Conductive properties of switchable photoluminescence thermosetting systems based on liquid crystals. *Langmuir: The ACS Journal of Surfaces and Colloids*, *26*(6), 4296–4302.

Tercjak, A., Gutierrez, J., Barud, H. S., Domeneguetti, R. R., & Ribeiro, S. J. L. (2015). Nano- and macroscale structural and mechanical properties of in situ synthesized bacterial cellulose/PEO-b-PPO-b-PEO biocomposites. *ACS Applied Materials & Interfaces*, *7*(7), 4142–4150.

Tercjak, A., Gutierrez, J., Barud, H. S., & Ribeiro, S. J. L. (2016). Switchable photoluminescence liquid crystal coated bacterial cellulose films with conductive response. *Carbohydrate Polymers*, *143*(5), 188–197.

Usov, I., Nyström, G., Adamcik, J., Handschin, S., Schütz, C., Fall, A., . . . & Mezzenga, R. (2015). Understanding nanocellulose chirality and structure-properties relationship at the single fibril level. *Nature Communications*, *6*, 7564.

Zhou, J., Collard, D. M., Park, J. O., & Srinivasarao, M. (2002). Control of the anchoring behavior of polymer-dispersed liquid crystals: Effect of branching in the side chains of polyacrylates. *Journal of the American Chemical Society*, 124.

dos Santos, M. V., Dominguez, C. T., Schiavon, J. V., Barud, H. S., de Melo, L. S. A., Ribeiro, S. J. L., . . . & de Araújo, C. B. (2014). Random laser action from flexible biocellulose-based device. *Journal of Applied Physics*, *115*(8), 83108.